The Impact of Ocean Initial Conditions on ENSO Forecasting with a Coupled Model

A. ROSATI, K. MIYAKODA, AND R. GUDGEL

Geophysical Fluid Dynamics Laboratory/NOAA, Princeton University, Princeton, New Jersey

(Manuscript received 31 October 1994, in final form 12 April 1996)

ABSTRACT

A coupled atmosphere–ocean GCM (general circulation model) has been developed for climate predictions on seasonal to interannual timescales. The atmosphere model is a global spectral GCM T30L18 and the ocean model is global on a 1° grid. Initial conditions for the atmosphere were obtained from National Meteorological Center (now known as the National Centers for Environmental Prediction) analyses, while those for the ocean came from three ocean data assimilation (DA) systems. One system is a four-dimensional DA scheme that uses conventional SST observations and vertical temperature profiles inserted into the ocean model and is forced from winds from an operational analysis. The other two initialization schemes are based on the coupled model, both nudging the surface temperature toward observed SSTs and one nudging surface winds from an operational analysis. All three systems were run from 1979 to 1988, saving the state of the ocean every month, thus initial conditions may be obtained for any month during this period. The ocean heat content from the three systems was examined, and it was found that a strong lag correlation between Nino-3 SST anomalies and equatorial thermocline displacements exists. This suggests that, based on subsurface temperature field only, eastern tropical Pacific SST changes are possibly predictable at lead times of a year or more. It is this ''memory'' that is the physical basis for ENSO predictions.

Using the coupled GCM, 13-month forecasts were made for seven January and seven July cases, focusing on ENSO (El Niño–Southern Oscillation) prediction. The forecasts, whose ocean initial conditions contained subsurface thermal data, were successful in predicting the two El Niño and two La Niña events during the decade, whereas the forecasts that utilized ocean initial conditions from the coupled model that were nudged toward surface wind fields and SST only, failed to predict the events. Despite the coupled model's poor simulation of the annual cycle in the tropical Pacific, the ENSO forecasts from the full DA were remarkably good.

1. Introduction

A major contributor to climate variability, on a wide range of timescales, is air–sea interaction. The El Niño–Southern Oscillation (ENSO) phenomenon, as a coupled oscillation of the tropical Pacific Ocean and the tropical atmosphere, represents a very important air–sea interaction on the seasonal to interannual timescale. The prediction of ENSO along with its global climate anomalies is a major research effort in short-range climate forecasting. Simulation of ENSO using ocean models forced with observed winds and heat flux (e.g., Busalacchi et al. 1983; Philander and Seigel 1985; Rosati and Miyakoda 1988; Harrison 1989) and using atmospheric models forced with observed sea surface temperature (SST) (Lau 1985; Latif 1987; Stern and Miyakoda 1995) have been successful in capturing the prominent features of ENSO. These successes are the groundwork for the coupled atmosphere–ocean GCMs, wherein further insight into ENSO dynamics may be obtained. Neelin et al. (1992) review the status of a variety of coupled models. Statistical and dynamical models have demonstrated that skillful predictions for eastern equatorial Pacfic SST anomalies are possible, for up to a year (Cane et al. 1986; Barnett et al. 1993; Latif et al. 1993).

The large-scale climatic variability associated with ENSO is tied to the slow oscillatory phenomena of the coupled atmosphere–ocean system in the Tropics. The ''memory'' (inertia) of this system resides in the upper ocean (< 250 m), which has a much longer timescale than the atmosphere. The importance of the role the internal ocean dynamics plays in the tropical Pacific has been discussed by Wyrtki (1985) and culminates in the delayed oscillator concept of Schopf and Suarez (1988) (see Graham and White 1988; Battisti 1988). The coupled system evolves from an initial state determined primarily by the thermal state of the upper ocean. The importance of how this initial state is represented, and how it impacts on coupled model ENSO forecasts, is the focus of this paper. A large effort in developing ocean data assimilation schemes to produce analyses that accurately represent the subsurface thermal structure has been made. This study contrasts the effects of analyses that use wind forcing only and analyses that combine wind forcing and subsurface data.

Corresponding author address: Dr. Anthony Rosati, Geophysical Fluid Dynamics Laboratory/NOAA, Princeton University, Forrestal Campus, P.O. Box 308, Princeton, NJ 08542.
E-mail: ar@gfdl.gov

This paper explores the forecast ability of a coupled GCM with varying ocean initial conditions. Section 2 describes the forcasting system, which includes the atmosphere and ocean models, and ocean data assimilation schemes. The upper-ocean heat content as the source of ''memory'' for the forecasts is examined in section 3. In section 4 the forecast skill is assessed and section 5 demonstrates the model's ability to capture the evolution of a warm and cold ENSO event. The conclusions are stated in section 6.

2. Forecasting system

In general, a forecasting system consists of a forecasting model and a method to initialize the model. For the coupled system, initial conditions for both the atmospere model and the ocean model are needed.

a. Atmosphere model

The atmosphere model used in this study is a global spectral GCM (Gordon and Stern 1982). The horizontal resolution is T30, which is the spectral triangular truncation at zonal wavenumber 30, corresponding to a Gaussian grid of approximatly 4.0° longitude by 4.0° latitude and the vertical resolution is L18 or 18 levels. The major physical parameterizations include a *bucket* hydrology over land; orographic gravity wave drag; large-scale condensation and moist convective adjustment (both using a condensation criteria of 100%); shallow convection, cloud prediction [interactive with radiation, Gordon (1992)]; radiative transfer (12-h averaged), which varies seasonally; stability dependent vertical eddy fluxes of heat, momentum, and moisture throughout the surface layer, planetary boundary layer, and free atmosphere (''E'' physics as described in Sirutis and Miyakoda 1990); and $k\nabla^4$ horizontal diffusion. The orography has been treated by a Gibbs oscillation reduction method (Navarra et al. 1994). This model with simpler physics and varying resolutions has been shown to be viable for extended range prediction at the monthly timescale (Stern and Miyakoda 1989), although systematic biases still contribute significantly to the error fields. As a precursor study to the fully coupled system, Stern and Miyakoda (1995) used a global SST dataset as boundary forcing for the atmospheric model, as described above, and generated an ensemble of GCM integrations to examine reproducibility as related to the feasibility of seasonal forecasts.

b. Ocean model

The configuration of the ocean model is the same as described in Rosati and Miyakoda (1988). The model equations are solved on a nearly global grid with realistic bottom topography (Bryan 1969; Cox 1984) using the modular ocean model (MOM) version as described in Pacanowski et al. (1991). The horizontal resolution is 1.0° longitude by 1.0° latitude except within the equatorial band of 10°N–10°S where the meridional resolution is 1/3°. This increased resolution within the equatorial zone is designed to resolve the strong SST gradient and oceanic internal waves, which may play a crucial role for the El Niño processes (see Busalacchi and O'Brien 1980; Busalacchi et al. 1983; Philander and Seigel 1985). The vertical resolution is 15 unequally spaced levels with most of the levels skewed toward the upper ocean above 500 m (Derber and Rosati 1989). The major physical parameterizations include penetration of solar insolation to the ocean subsurface, vertical mixing formulated after the turbulence closure scheme level 2.5 of Mellor–Yamada (1974; nearly the same scheme used by the atmospheric model), and horizontal mixing adapted from the Smagorinsky nonlinear viscosity (Smagorinsky 1963). This version of the model was forced with observed winds and heat flux and was found capable of producing realistic interannual variability of the ocean (Rosati and Miyakoda 1988).

c. The coupling

The atmosphere and ocean models are coupled as follows. The atmosphere is run for 12 h with a 20-min time step. The 12-h averages of wind stress, heat flux, and precipitation minus evaporation are saved to force the ocean model. Then the ocean model is run for 12 h with 1- and 2-h time steps for momentum and temperature/salinity, respectively, and returns the 12-h averaged SST to be used in the subsequent 12-h integration of the atmospheric model.

Even though the atmosphere and ocean models demonstrate good performance individually, when coupled and run ''free,'' without observed boundary forcing, there is no guarantee that the models will not drift to some new climate state where they can establish an equilibrium. The systematic bias was fairly large in the preliminary studies of the coupled model (Sirutis and Miyakoda 1989; Miyakoda et al. 1989, 1990). The model tended to have a cold bias that was particularly evident over the western tropical Pacific where the SST warm pool was colder by 2°–4°C. The trades were excessively strong in the eastern Pacific. For the most part these same systematic biases exist in the present version; however, a heuristic correction was made. After examination of the heatflux components it was found that the evaporative term was too large and so the evaporation coefficient C_E was reduced uniformly by 10% over the ocean surface.

d. Initial conditions

Experience in weather forecasting suggests that when the influence of initial conditions fades away as a prediction proceeds, predictability decreases (e.g., Arpe et al. 1985). If this is true for the coupled system as well, the presence of adequate information in the initial con-

ditions is of paramount importance for the seasonal forecasts. For this seasonal timescale, the assumption is that the long-term memory of the coupled atmosphere–ocean system is provided by the ocean, thus particular care must be taken in initializing the ocean model.

In this study, the initial conditions for the atmospheric component are obtained using National Meteorological Center (NMC, now known as the National Centers for Environmental Prediction) analysis. The main focus of this paper will be to ascertain the impact of ocean initial conditions on the forecasts, and so we will try three different data assimilation (DA) schemes to initialize the ocean. Knowing that neither the model nor the observations are perfect, the goal of DA is to estimate optimally the past and present states with an imperfect model and noisy observations. The description of the DA systems used in this study follows.

1) FULL DATA ASSIMILATION

As the first step toward the coupled model prediction system, an ocean DA scheme was developed by Derber and Rosati (1989). Observed data were continuously inserted into the ocean model by applying a correction to the forecast temperature field at every model time step. The spatial objective analysis technique is based on the statistical interpolation (optimal interpolation) analysis scheme of Gandin (1963). The method is based on a variational principle, in which the ocean model solutions are used as the first guess for temperature and the final analysis is determined by the inserted oceanographic data in such a way that a functional be statistically minimal. The functional is represented by, first, the difference between the observations and the corrected temperature field, and, second, the difference between the corrected temperature field and the first guess, in which the observational error is taken into consideration. The functional is minimized using a conjugate gradient algorithm.

The upper boundary conditions of the ocean GCM are specified by surface wind stress, atmospheric heat flux, and moisture flux, which were computed using the twice daily NMC operational analysis, and also incoming shortwave and net longwave radiation, given by seasonally varying climatologies.

This system has been implemented using a long time series of ocean data analysis. The period of the assimilation is 10 years from January 1979 to December 1988 (Rosati et al. 1994—hereafter referred to as RGM94). During this decade, various national and international projects of data acquisition and processing were carried out. For ocean surface temperature data, COADS (Comprehensive Ocean–Atmosphere Data Set, based on ships of opportunity) was taken. The subsurface temperature data (from XBTs temperature profiles) was an amalgamation of datasets from NODC (the National Oceanic Data Center), U.S. Navy's MOODS (Master Oceanic Observation Data Set), and TOGA (Tropical Ocean Global Atmosphere project). The ocean model is integrated forward in time while these data are continuously assimilated by the model, serving to produce an analysis and initial conditions anywhere along the 10-yr period. This is essentially the same system used by the coupled model project at NMC (Ji et al. 1994).

It should be noted that the oceanic data inserted into the model has been limited to temperature data. Although this is done for practical reasons, that is, there is no extensive array of velocity measurements, studies by Philander et al. (1987), Anderson and Moore (1989), and Hao and Ghil (1994) have shown the relative usefulness of thermal data over velocity data. This difference in importance follows since the most important consequence of the equatorial ocean's adjustment to wind stress is the balance between east–west pressure gradient and zonal wind. Therefore, the assimilation of temperature observations would define the pressure gradient and this information would be transferred to the model dynamics. In other parts of the ocean where the flow is primarily geostrophic, the insertion of only mass data would also be justified.

2) SURFACE DATA ASSIMILATIONS

In addition to the full DA, there are simpler DA methods, that is, Newtonian nudging of surface boundary conditions. If this method proves to be comparable to the full DA in terms of the analysis quality and forecasting skill, the nudging technique may be a viable option for the generation of initial conditions.

The nudging technique is applied to the coupled air–sea model in two ways. The first is to nudge the ocean model's surface temperature toward observations. The second is to nudge SST and the surface wind stress toward observations. Both methods are run for the period 1979–88 and attempt to address the adjustment issue for initializing the coupled model. The idea is that surface winds generated by the atmosphere model, influenced from the observed SST field, would initialize subsurface fields that would be in balance with the atmospheric model forcing, and therefore the models would not be shocked when coupled. Specifically, the east–west pressure gradient along the equatorial ocean would be in balance and defined by the atmospheric model's zonal winds and hence would not need to come into rapid adjustment to a new wind field. Essentially this method initializes the ocean model from the observed SST field. The second scheme uses the observed wind field forcing and SST field to initialize the subsurface.

The SST nudging: taking the coupled model, the thermodynamic equation for the upper-most layer of ocean model is modified by adding Newtonian nudging term; that is,

$$\frac{\partial T}{\partial t} \cdots = -\lambda(T - T_{\text{obs}}), \tag{2.1}$$

where T is the ocean temperature at level 1, T_{obs} is the observed SST, and λ is the Newtonian damping coefficient, (3 day)$^{-1}$. Here, T_{obs} is the monthly mean SST analysis of Reynolds (1982, 1988).

The SST–wind nudging: taking the same coupled air–sea model, two equations are modified. One is the equation of oceanic temperature, that is, the same as Eq. (2.1). The other is the equation of momentum in the lowest layer of the atmospheric GCM; that is,

$$\frac{\partial}{\partial_t}\mathbf{V} \cdots = -\mu\ (\mathbf{V} - \mathbf{V}_{obs}), \tag{2.2}$$

where $\mathbf{V}$ is the wind vector, the term $-\mu(\mathbf{V} - \mathbf{V}_{obs})$ is the Newtonian nudging coefficient, μ is the damping coefficient, (1 h)$^{-1}$, and $\mathbf{V}_{obs}$ is the observed wind vector. The observed winds are the same as used in the full DA, taken from NMC analysis, and the nudging terms are applied over the ocean surface, excluding land. This approach of using past wind fields to precondition the ocean model is carried on by several ENSO prediction groups (Inoue and O'Brien 1984; Cane et al. 1986; Latif and Flugel 1991). Chen et al. (1997) showed that initial conditions obtained from the coupled model nudged toward FSU wind stress improved their forcasts. They attributed the success of the scheme to its consideration of coupling, and the reduction of ''initialization shock'' in the transition from hindcast to forecast mode. Their value of the nudging coefficient was a function of latitude as opposed to the one used in the S-DA1, which is a constant.

In summary, a hierarchy of DA schemes to produce initial conditions from ocean analysis were run and are described as follows:

1) Ocean model—full DA; uses observed SST; observed surface winds; and subsurfasce thermal data.
2) Coupled model—SST–wind nudging; uses observed SST; observed surface winds.
3) Coupled model—SST nudging; uses observed SST.

The forecasts run from these three initial conditions are referred to as the F-DA, S-DA1, and S-DA2, respectively.

3. Upper-ocean heat content

An important component of the coupled ocean–atmosphere system on the interannual timescale is upper-ocean heat content. Many studies have shown (e.g., Zebiak and Cane 1987; Harrison 1989; Battisti 1988; Graham and White 1988; Chao and Philander 1993; Neelin et al. 1992) that fluctuations in upper-ocean heat content are both systematic and significant in the evolution of ENSO. To quantize this character, the heat content is calculated by

$$\text{heat content} = \int_{-248\ \text{m}}^{0} \rho C_p T\, dz, \tag{3.1}$$

where 248-m depth is taken to include the thermocline level around the equatorial Pacific, and it corresponds to the 11th level from the surface in the ocean model, $\rho = 1.02$ g cm^{-3} and $c_p = 4.187$ J g^{-1} K^{-1}.

Figure 1 shows Hovmöller diagrams of heat content along the equator for temperature nudging at the right, temperature-wind nudging in the middle, and full DA on the left. The two nudging cases, the middle and the right panels in Fig. 1, do not show good agreement with each other. The temperature nudging case shows a pronounced annual cycle in the eastern part of the basin. Although this is a feature of the SST, observed annual variations in thermocline depth are weak, and, therefore, the annual cycle in heat content for this case is unrealistic. In the western part of the basin, the temperature nudging case contains much more heat than the other two cases. What this reveals is the sensitivity of the subsurface thermal field to the wind field. In the temperature nudging case the winds that drove the ocean model were generated from the atmospheric model. Examination of the model winds showed stronger than observed westerlies in the western equatorial Pacific during DJF. This resulted in convergence at the equator and caused downwelling, which influxed a large amount of heat into the ocean. This was possible since the model surface temperature was being forced to observed SSTs and therefore there was a positive heat flux into the ocean. In the coupled system, this wind bias increases evaporation and reduces the heat flux into the ocean resulting in SSTs that are too cold. When the NMC analysis wind field is used, the systematic westerly bias is removed and a more reasonable heat content is simulated, as shown in the temperature–wind nudging and DA cases. It was also found that the atmospheric model had a bias toward trade winds that were too strong. Without the SST nudging, this would have resulted in increased upwelling and SSTs that would be too cold in the central and eastern Pacific. However, with the flux adjustment enormous amounts of heat had to be fluxed into the ocean model to maintain the observed annual cycle of SST due to the systematic error in the model wind field. This resulted in the pronounced annual cycle in the heat content. Looking at the heat content over the central Pacific, a much tighter gradient may be observed in the DA as opposed to the other two cases. This shows that the ocean model produces too diffuse a thermocline, and that this bias may be alleviated by the addition of subsurface data in the DA. It would appear that for the present system subsurface thermal data are necessary and that using only the wind fields, either from the model or analysis, is not adequate to derive the ocean subsurface thermal structure.

Figure 2 shows time–longitude diagrams of the heat content anomalies along the equator, in the Pacific, from 1981 to 1988. As in the previous figure, the left panel is the DA; the middle is the temperature–wind nudging; and the right is the temperature nudging. Where the total heat content showed distinct differences between the

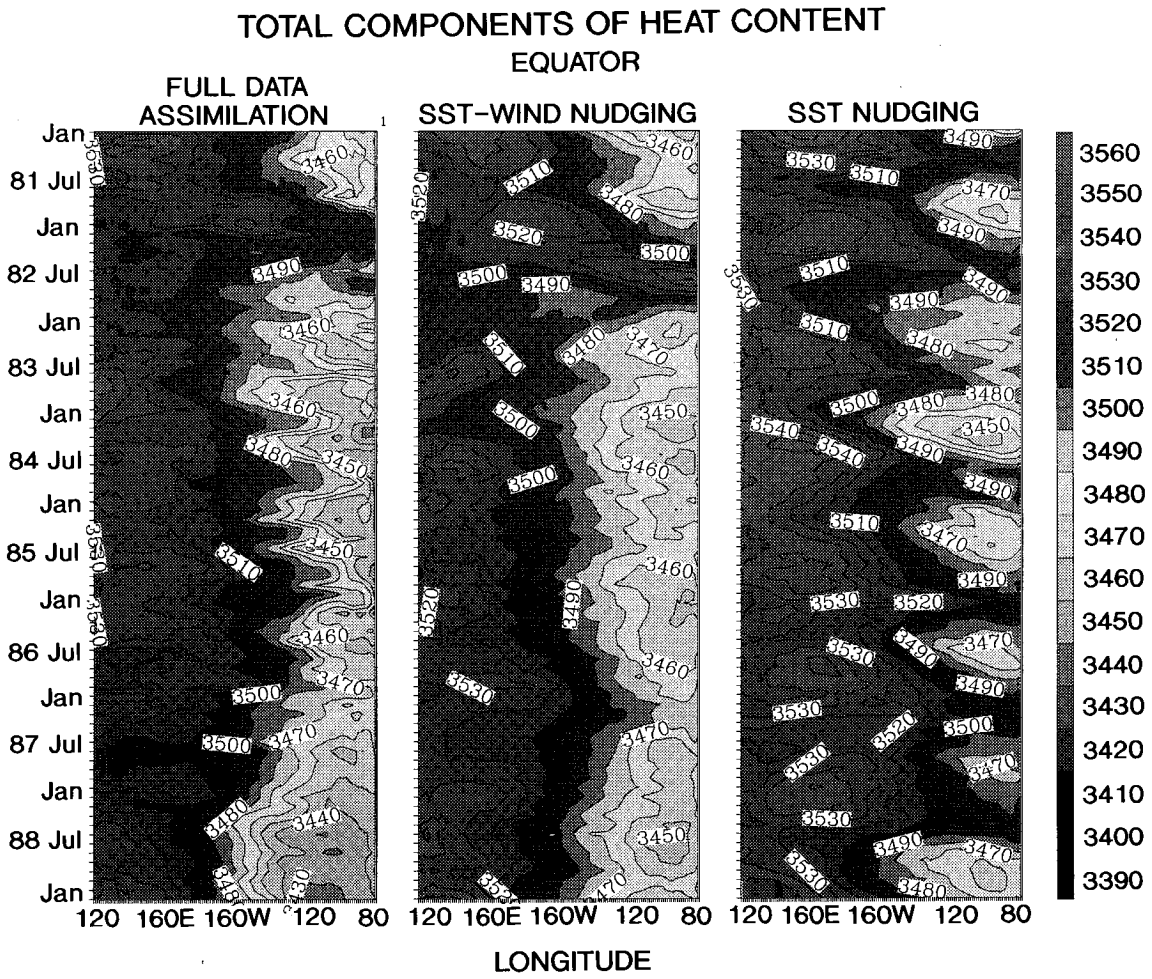

FIG. 1. Time–longitude diagrams of ocean heat content along the equator from the three DA systems. The contour interval is 10^9 J m^{-2}. The thick line is the 352 $\times$ 10^9 J m^{-2} contour. The regions greater than 352 $\times$ 10^9 J m^{-2} are stippled.

three assimilations, the anomalies, about their individual means, show that the interannual fluctuations of the thermocline are similar. The most pronounced feature in Fig. 2 is the two distinct episodes of El Niños and of La Niñas and show that these positive and negative anomalies of heat content propagate eastward. Comparison with SST anomalies (not shown here) shows the two El Niño signatures are evident; however, the 1986–87 event is more distinct in the SST anomalies than in the heat content anomalies. Further, for the whole period, the eastward propagation is dominant in the heat content, as opposed to some element of westward propagation in the SST. This coherence between SST anomalies and heat content anomalies appears to be essential to ENSO predictability. It would seem of paramount importance that the assimilation scheme, used to produce initial conditions for ENSO forecasting, must contain an accurate representation of the phase and amplitude of these propagating heat content anomalies.

The upper ocean is the main component active on the interannual timescale in the coupled ocean–atmosphere system. ENSO prediction models such as described in Inoue and O'Brien (1984), Cane et al. (1986), and Latif and Flugel (1991) use observed wind fields up to the initial forecast time to precondition the ocean as the only data that enters their predictions. The success of these models leads one to believe that the ocean acts as a filter on the wind stress to extract the interannual variability, which makes the coupled model less sensitive to the unpredictable components of the atmosphere. Latif and Graham (1992) showed that using the upper-ocean temperatures from an ocean GCM forced by observed winds as the predictors in a statistical model gives significantly better skill at lead times of 6 to 12 months compared to either persistence or the statistical model based on wind stress data only. Chao and Philander (1993) describe their results as a generalization of the ''delayed oscillator'' (Schopf and Suarez 1988) mechanism in which a superposition of many wave modes plays an important role in determining the delayed response of the ocean. The net effect of these waves is to modulate the equatorial heat content and

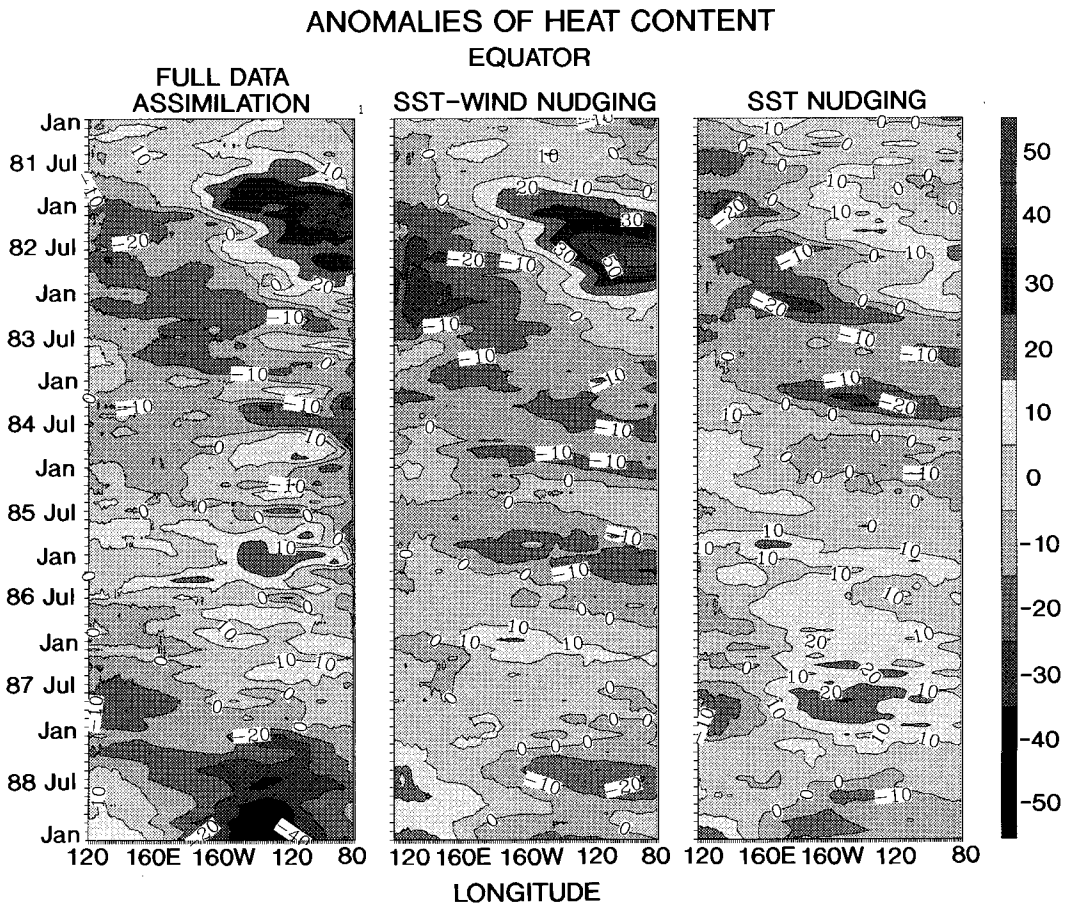

FIG. 2. Time–longitude diagrams of heat content anomalies along the equator from the three DA systems. The contour interval is 10×10^9 J m^{-2}. Regions greater than 10×10^9 J m^{-2} and less than -10×10^9 J m^{-2} are stippled differently.

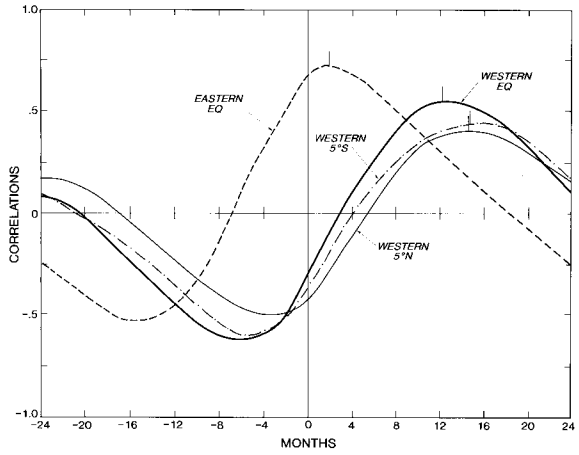

FIG. 3. Lag correlations of Nino-3 SST and ocean heat content anomalies for four different regions. Positive (negatve) lags indicate that SST lags (leads) heat content anomalies.

currents, effects that may then be amplified by the atmospheric feedback. It is the relatively long ''memory'' of the tropical Pacific Ocean (that there is at any moment a delayed oceanic response to earlier winds) that permits a continual oscillation and provides the physical basis for ENSO prediction. Since the ''memory'' is associated with thermocline displacements, then it would follow that the expression of this redistribution of heat should manifest itself through SST. Using the DA to demonstrate this relationship, a correlation analysis of heat content anomalies with SST anomalies in the Nino-3 region (5°N–5°S, 150°–90°W) was made (Fig. 3). Similar to Latif and Graham (1992), heat content anomalies over key regions were selected for the analysis: 1) the eastern equatorial Pacific (0°, 160°–80°W); 2) the western equatorial Pacific (0°, 140°E–160°W); 3) the northern west Pacific (5°N, 140°E–160°W); and 4) the southern west Pacific (5°S, 140°E–160°W).

Figure 3 shows a maximum correlation between Nino-3 SST changes and eastern equatorial thermocline displacements at 2-month lag, indicating the sensitivity to subsurface thermal changes. The maximum, at the

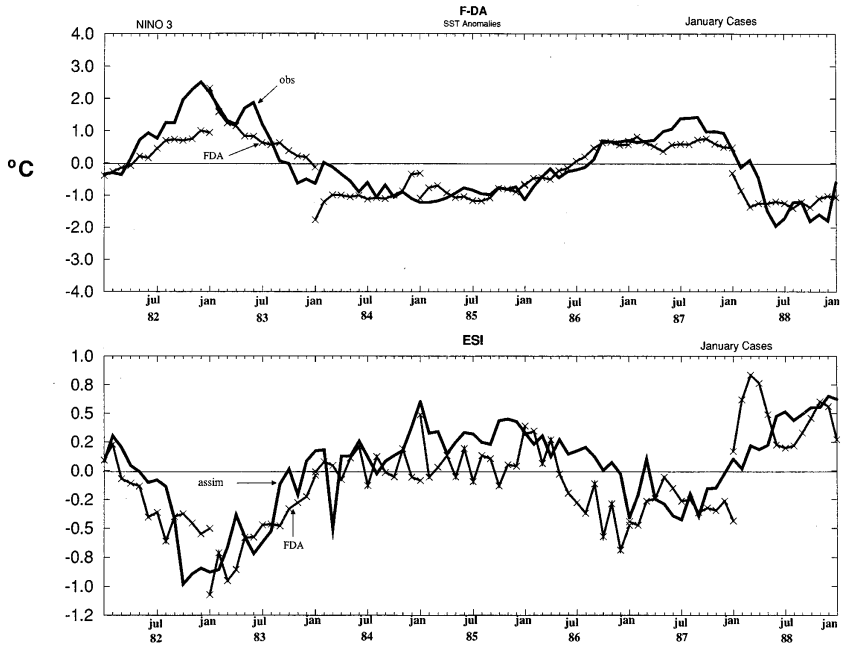

FIG. 4. Nino-3 SST anomalies (top panel) and ESI (bottom panel). The thick lines are from analyses. The crosses are the coupled model forecast results started in January for the F-DA cases.

western equatorial Pacific is at 12-month lag, and the off-equatorial region is at 16-month lag. This shift in the correlation maximum to larger lags shows the propagation of heat content anomalies from off the equator into the equatorial waveguide and then propagating eastward, characteristic of the ''delayed oscillator'' mode, the physics of which are substantially different than those expected from Kelvin wave dynamics (see Barnett et al. 1991). This suggests that, based on subsurface data only, eastern equatorial Pacific SST changes are possibly predictable at lead times of a year or more. It then follows that using an ocean model, capable of propagating these heat content anomalies, with a realistic initial state coupled with an atmospheric model, forecasts of eastern equatorial Pacific SST anomalies are possible. However, if this ''memory'' that the ocean has to earlier winds is misrepresented, possibly due to model and/or forcing errors, then the initial state of the ocean model, used in a coupled forecast mode, could be in error. There would be propagation of thermocline displacements, but since the initial heat content would be different from observations, they would be incorrect. The basis of this study is to explore the impact of various ocean initial conditions on the forecast.

A convenient way to represent zonal mean heat content anomaly along the equator is to define an ENSO index such that

$$\mathrm{ESI} = \frac{D_W - D_E}{110 - 1},$$

where D is the depth of the 20°C isotherm, and D_W and D_E are the depths at 160°E and 90°W, respectively. Here, 110 m corresponds to the climatological mean value of $D_W - D_E$, that is, $160 - 50 = 110$. When ESI is negative (positive), the index indicates a shoaling (deepening) of the thermocline in the west and a deepening (shoaling) in the east corresponding to a warm (cold) event. The ESI is essentially the zonal mean of Fig. 2; the advantage of this index is that it allows the computation of zonal mean heat content anomalies without having to compute a climatology.

4. Forecast results

The forecasts consist of seven 13-month cases starting from January or July every year for the period 1982–88. The time of the initial conditions is 0000 UTC of the first day of January or July. Each January forecast is run from three versions of ocean initial conditions—F-DA, S-DA1, and S-DA2—as described above, but the July forecasts were run only from the F-DA version. This time period included two warm events and two cold events.

The results of the seven January forecasts, initialized from F-DA and S-DA2, are displayed in Figs. 4 and 5. For each month of the forecasts, the monthly mean SST anomaly was computed over the Nino-3 region and is shown in the upper panels. The anomaly was calculated by creating a forecast climatology from the ensemble of cases and subtracting it from the individual forecast. The lower panels are the zonal mean heat content anomaly index or ENSO index, that is, ESI. The continuous

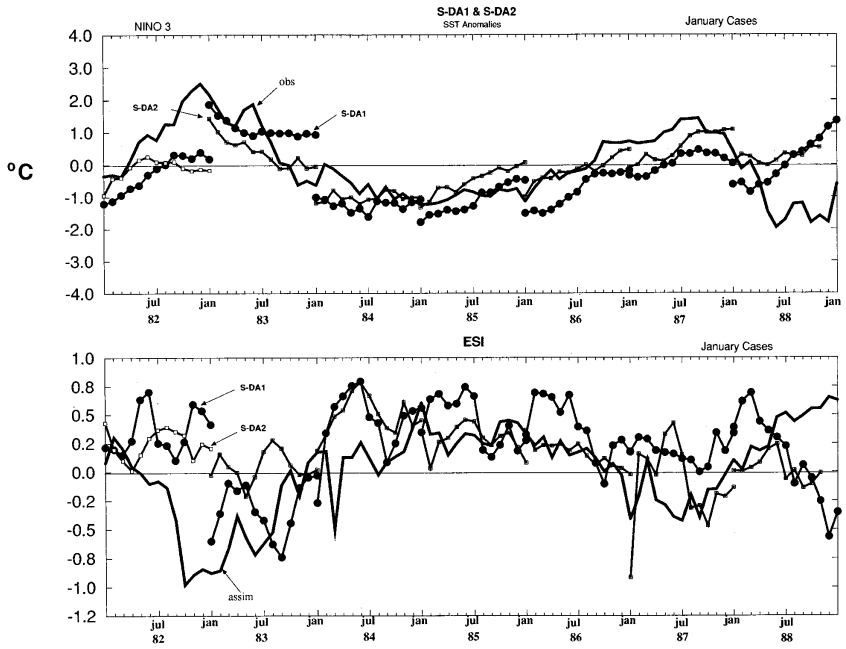

FIG. 5. The same as Fig. 4 but for the S-DA1 and S-DA2 cases.

thick line curves are observed SST anomalies, after Reynolds (1988), and the ESI from the full DA (Fig. 2). The thin line curves with crosses are the SST and ESI anomalies from the seven forecast cases, each run for 13 months. The terminal points of the 13 months are indicated by black dots with crosses. Figure 6 is similar but for July cases. Although the forecasts started from the DA, the first month does not agree exactly because it is a monthly mean of the forecast.

The SST forecasts, shown in the upper panel of Fig. 4, agree quite well in capturing the temperature increases in 1982/83 and 1986/87 and also the temperature decreases in 1983/84 and 1987/88. During 1984/85, when the anomalies had little change, the forecasts again did well. The lower panel is the ESI and it should be noted how well it correlates with the Nino-3 SST anomaly, as discussed in Fig. 3. Since we believe the key to the SST forecast lies in the proper redistribution of the

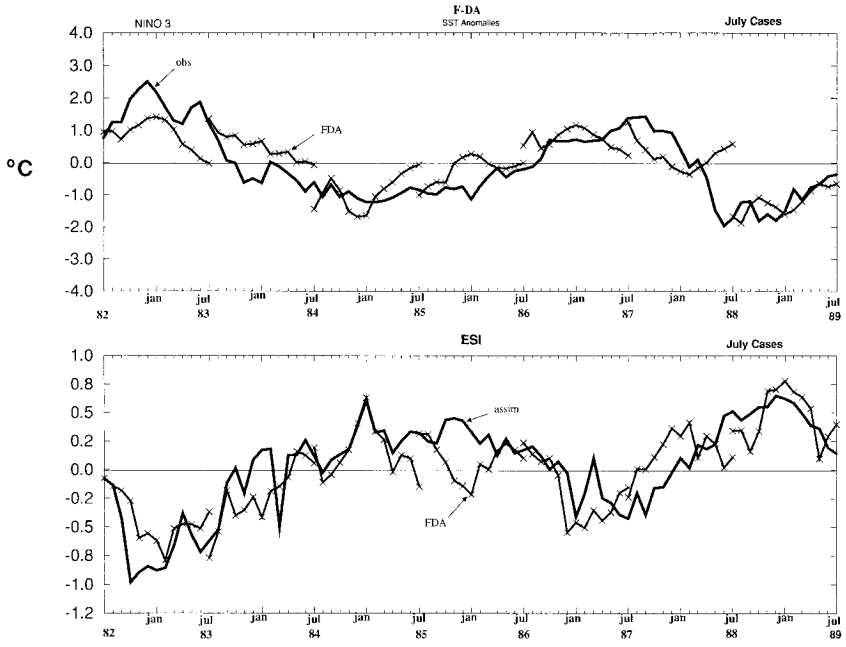

FIG. 6. The same as Fig. 4 but for July.

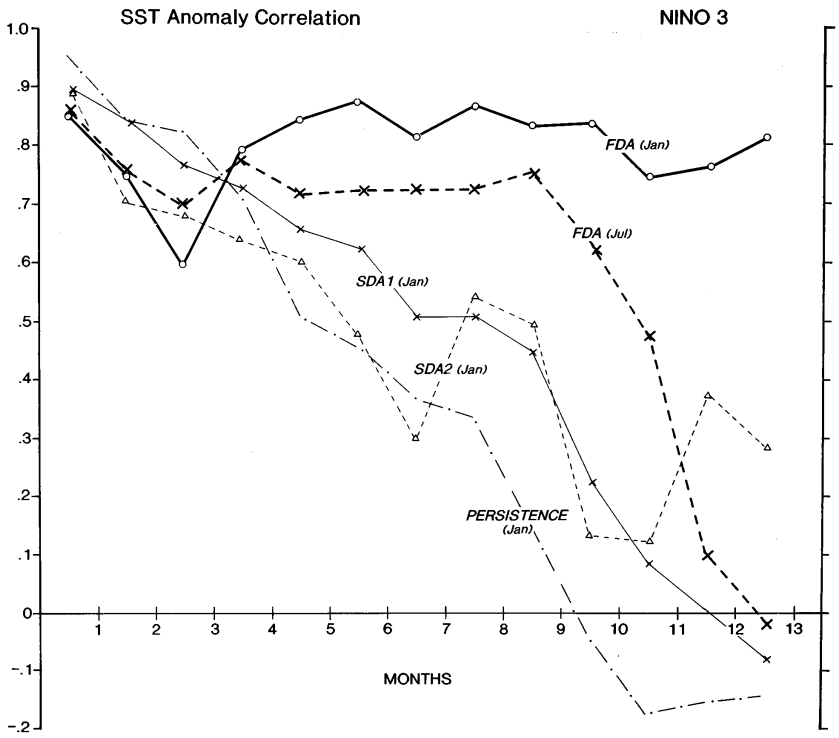

FIG. 7. Nino-3 SST anomaly correlations for the ensemble of F-DA and S-DA cases over the 13-month forecast period. Persistence is also shown for comparison.

ocean heat content, we compare the forecast zonal mean heat content anomaly with the DA. The forecasted ESI seems to capture the anomalous behavior of the heat content associated with the rise and fall of the thermocline and hence the good SST prediction. Figure 6 contains the results for the cases starting in July. The SST and ESI forecasts seem to begin well but do not have the same skill as the January cases, particularly for the last 5 months (spring onward). Forecasts where the ocean is initialized by the S-DA1 and S-DA2 (Fig. 5) show little skill, with the 1982/83 cases going cold and the remaining cases going warm. A summary plot of the results from all the cases is Fig.7, showing correlation coefficients from the ensemble of forecasts. The F-DA cases do the best with F-DA(JAN) having approximately 0.8 (except for March) and rms error of 0.56°C (not shown) for the whole 13-month period, wheras the F-DA(JUL) exhibits decreasing skill beginning in April and a mean rms error of 0.75°C. The S-DA1 (rms 1.1°C) is marginally better than S-DA2 (rms 0.84°C) for the first seven months. Beyond 3 months, all but S-DA2 of the forecast cases do better than persistence. The rapid decrease in correlation over the first 3 months is consistent with the fast error growth as noted by Blumenthal (1991) and discussed by Latif et al. (1992). These results show that the use of subsurface thermal data in preconditioning the ocean (F-DA) lead to better equatorial SST anomaly forecasts as opposed to preconditioning the ocean only from wind and SST data (S-DA1 and S-DA2). The coupled model experiments described by Zebiak and Cane (1987) also demonstrated the important role of mean equatorial heat content by showing that interannual oscillations did not occur if the thermocline was too shallow. It should be pointed out, however, that other investigators using FSU winds only, in total or anomalies, to initialize the ocean have had greater success than our S-DA1 case (Chen et al. 1996; Latif et al. 1993).

Two additional F-DA forecasts were made, for the contrasting 1987 warm case and the 1988 cold case, wherein the atmospheric initial conditions were altered by replacing each year with the other. The results showed little change in the predicted SST anomalies, further emphasizing the dominant role of the ocean ''memory.'' These results are hardly conclusive; on the other hand had these experiments not demonstrated this, our expectations for seasonal to interannual predictions would be greatly reduced. Also the impact of some low-frequency signal, for example, QBO, needs to be addressed more completely.

SST anomaly correlations over the world oceans (Fig. 8) are computed where the observed SST anomalies are again from Reynolds's (1988) analysis. Correlations are obtained from months 4–9 of the combined January and July F-DA forecast cases. The highest correlation region is located in the eastern and central equatorial Pacific (>0.75). The other regions of high correlation are found

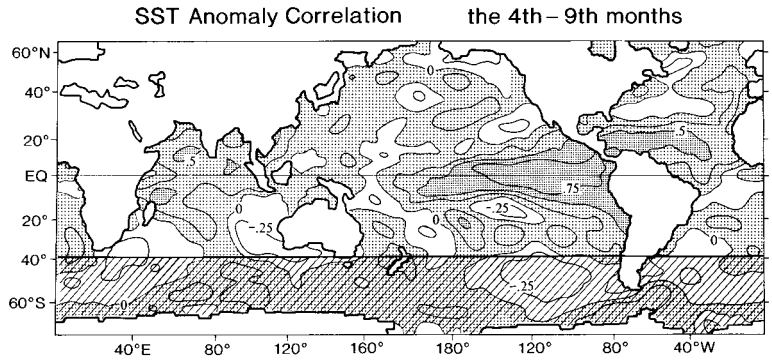

FIG. 8. SST anomaly correlation for months 4–9 for the ensemble of F-DA cases (14). Cross hatching poleward of 40°S indicates observations are sparse and rely primarily on climatology. Positive values are stippled with values greater than 0.5 stippled finer.

over the tropical Atlantic (>0.5) and over the Indian Ocean (>0.5).

It should be pointed out that coupled model's annual cycle along the equator shows considerable climate drift (Fig. 9). Comparing Reynolds's SST climatology to the forecast model's climatology, obtained from the mean of the ensemble of F-DA cases, the warm pool in the west cools by 2°–4°C and the amplitude and phase of the seasonal cycle is poor. Nevertheless, despite this deficiency in simulating the tropical Pacific annual cycle, the F-DA anomaly forecasts demonstrated remarkable skill. As has been discussed by Neelin et al. (1992) and Latif et al. (1993), the presence or absence of interannual variability does not appear to depend importantly on climate drift; also coupled GCMs that simulate a realistic mean climatology do not necessarily simulate interannual variability properly. For other regions of the World Ocean the seasonal cycle is well simulated.

5. Evolution of two ENSO predictions

To evaluate the impact of oceanic initial conditions on the predictions, two cases, from the 1982–88 ensemble, are selected and studied. Each one starts from 1 January initial conditions and the forecast period is 13 months. The cases were chosen to demonstrate the model's predictive capability for a warm and a cold event.

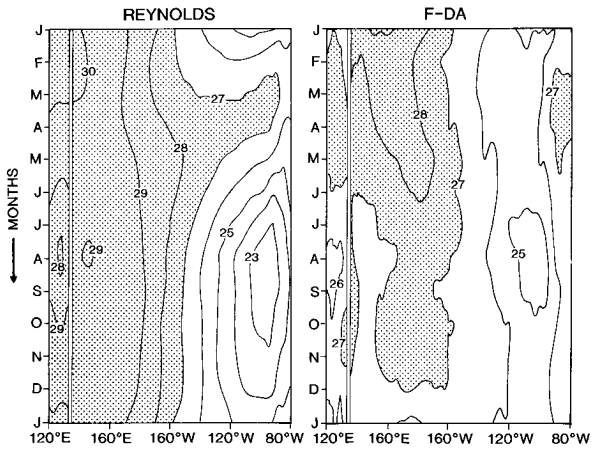

FIG. 9. Time–longitude diagrams, along the equator, of SST climatologies from Reynolds analysis and the mean of the F-DA cases.

a. The warm event (1982–83 El Niño)

The details of the evolution of the monthly mean subsurface thermal structure within the model predictions is provided in longitude–depth sections at the equator (Figs. 10 and 11). Here the DA analysis is taken as the best representation we have to the real ocean and forecasts are compared to it as reference. Examining the DA (top of Fig. 10), in January 1982, we see the characteristic deep warm pool in the west and cold upwelled water in the east. As we follow the slope of the thermocline in time, we see a distinct shoaling in the west and a deepening in the east, and by January 1983 a total redistribution of heat from west to east. We would hope that the forecasts exhibit similar features. Looking at the FDA forecast case we see that the initial conditions show a very tight thermocline; however, as the forecast progresses, the thermocline becomes too diffuse as compared to the DA. This systematic error manifests itself in all of the ocean runs not constrained by observations. Both S-DA initial conditions show this bias. The temperature anomalies (Fig. 11) of the DA show a clear eastward propagation of heat content, and by January 1983 the west is negative and the east positive indicating the change in slope of the thermocline. The warming in the east is unprecedented. This evolution is successfully simulated by the F-DA, although the anomalies lack the amplitude of the DA. However, the S-DA1 and S-DA2 cases do not show the same changes in thermocline displacements and do not forecast El Niño. In fact the S-DA2 case even has warming in the west and cold in the east. It should be mentioned that the means from the ensemble of forecasts of each case were subtracted to produce the forecast anomalies.

Figure 12 shows the SST anomalies over the entire Pacific. The observations clearly show the warm waters

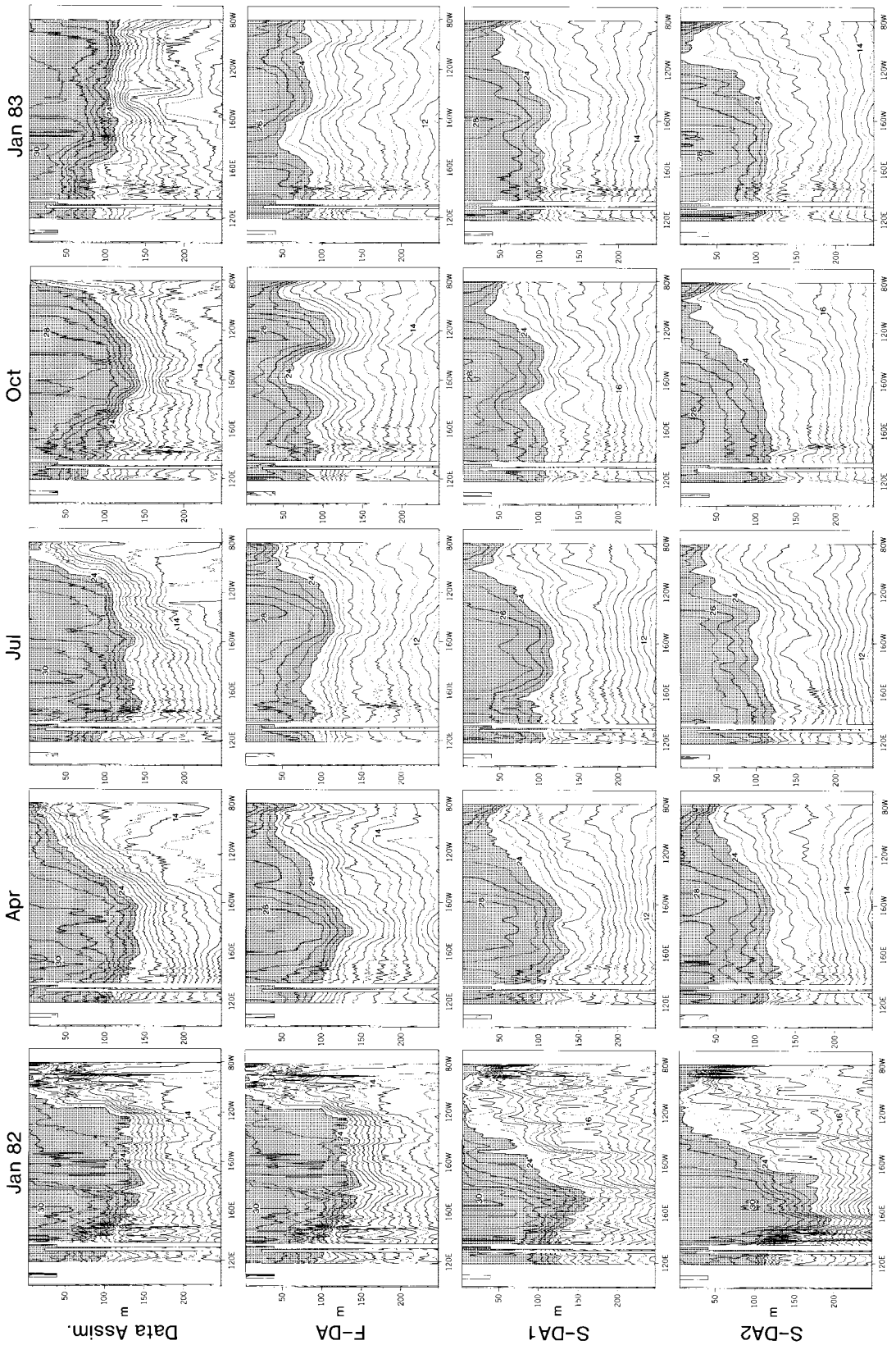

FIG. 10. East–west cross sections of temperature along the equator during 1982. The top row is the DA, the second to fourth rows are the forecasts from F-DA, S-DA1, and S-DA2, respectively. The contour interval is 1°C and values greater than 24°C are stippled.

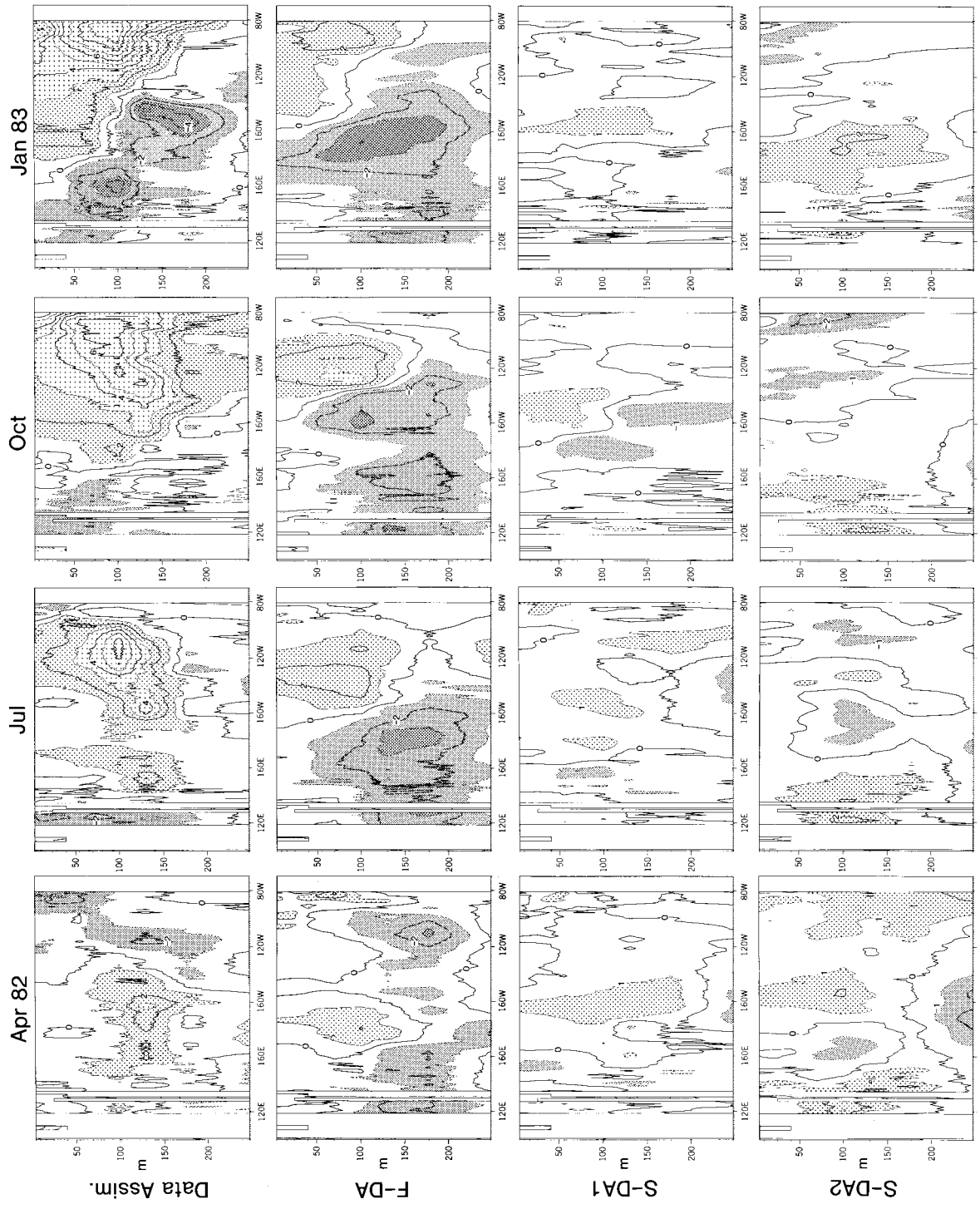

FIG. 11. The same as Fig. 10 but with anomalies. Positive anomalies greater than 1°C and negative anomalies less than −1°C are stippled.

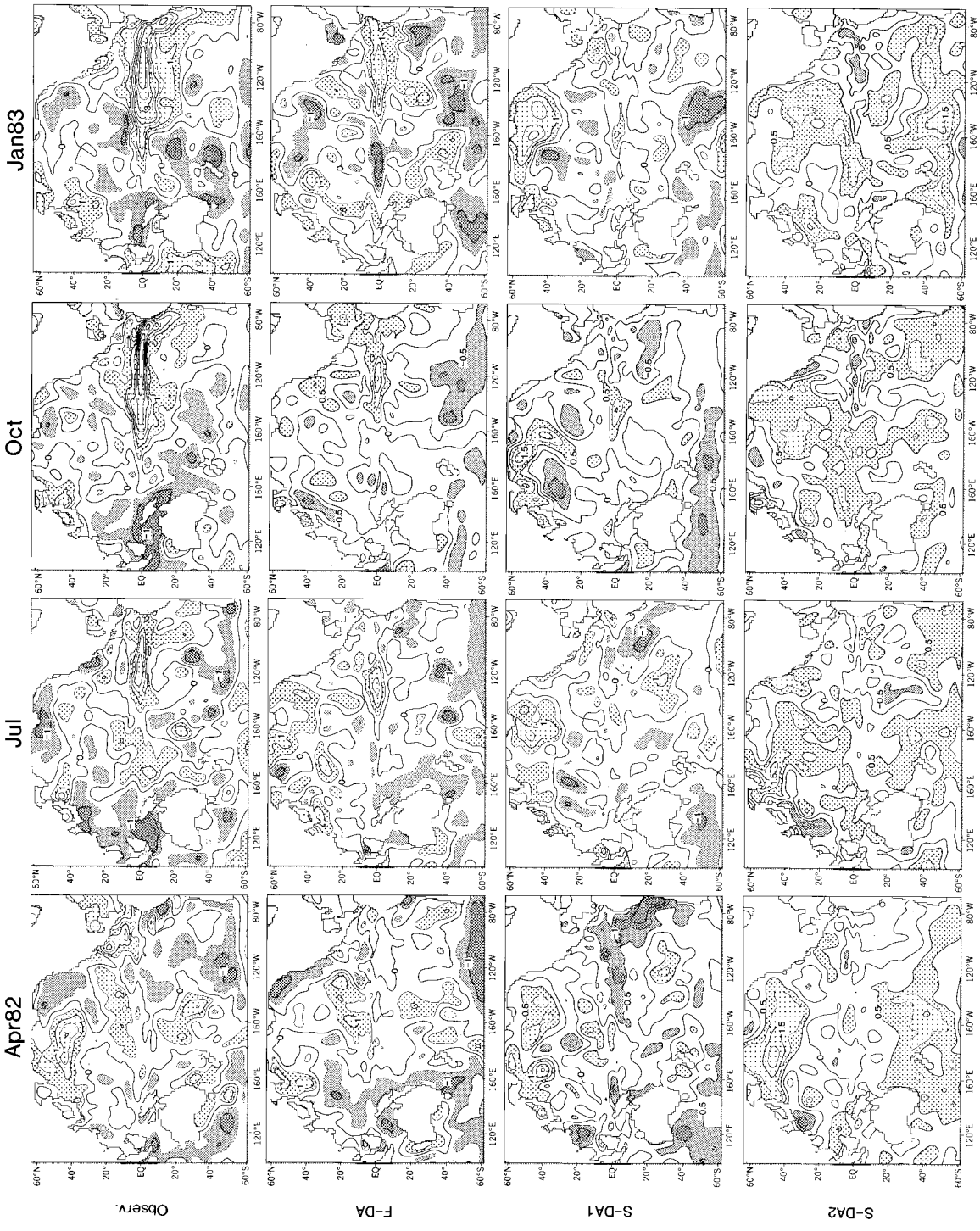

FIG. 12. SST anomaly maps over the Pacific basin for 1982. The rows are arranged as in Fig. 10. The contour interval is 1°C.

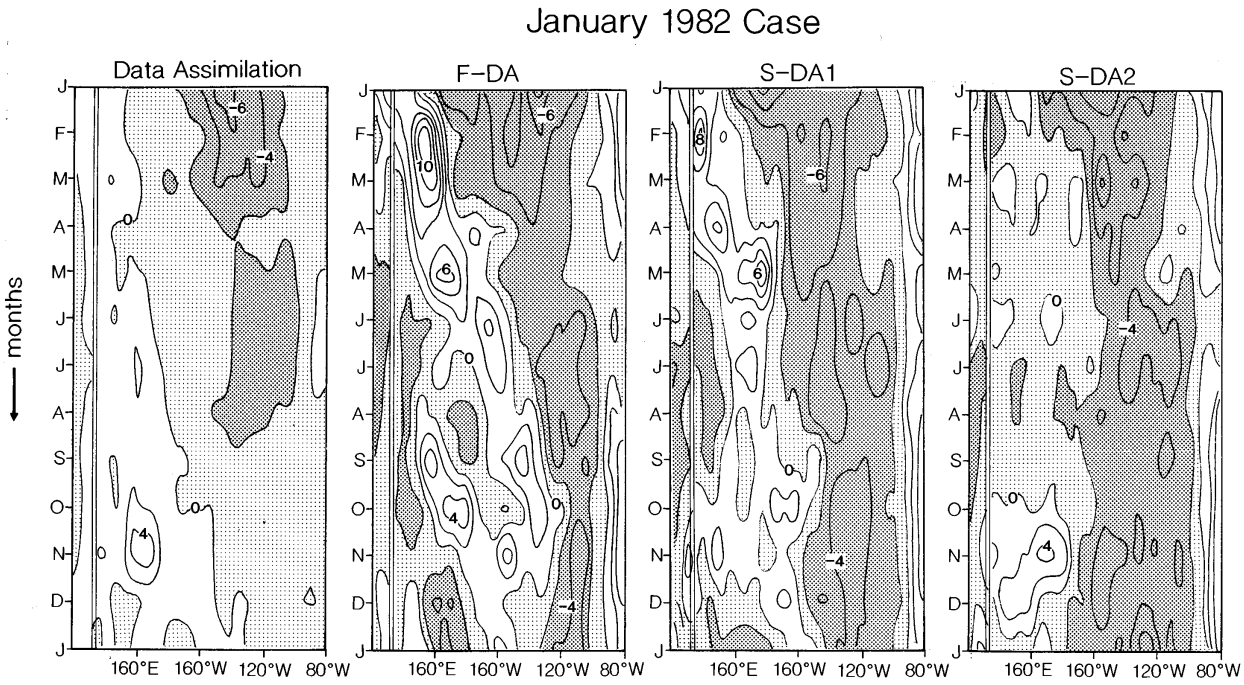

FIG. 13. Time–longitude diagrams of the zonal component of wind stress for 1982. The left-most panel is after NMC analysis. The remaining three panels are from the 1982 forecasts. Easterlies are stippled and the contour interval is 2 N m^{-2}.

in the central and eastern parts of the basin. The F-DA case predicted the warm SST anomaly, although it is too narrowly confined to the equator. The S-DA cases do not predict this warm event. The wind stress (Fig. 13) from the NMC analysis has westerlies that migrate from west to east; this feature is best represented in the F-DA forecast. The S-DA2 case even has strong easterlies, coinciding with the cold SSTs.

b. The cold event (1988–89 La Niña)

In the 1988 case (Fig. 14), the DA analysis shows east–west slope of the thermocline steepens in time, deepening in the west and shoaling in the east (upwelling colder than normal water in the east). The F-DA forecast simulates this evolution very well, while the S-DA forecasts fail totally and even swing into warm events. This feature is more evident in the anomaly fields in Fig. 15 where heat content anomaly in the east is cold and warm in the west, just the opposite of the 82 case, for the DA. Once again the F-DA case predicts this redistribution of heat although weak compared to the DA.

The observed SSTs in Fig. 16 show a dramatic development of the equatorial cold tongue as early as April in the east and then extending west across the basin. The F-DA forecast is successful in simulating the cold tongue; here again it is too narrowly confined to the equator. The S-DA forecasts fail and even contain erroneous warm water. The wind stress (Fig. 17) from the analysis has strong easterlies that persist throughout 1988. The F-DA best represents this feature, although there are also erroneous westerlies. The S-DA cases westerlies migrate eastward as in the El Niño case.

6. Conclusions

A coupled atmosphere–ocean GCM has been constructed. The atmosphere component is a T30L18 global spectral GCM. The ocean component is a global ocean GCM with 1° horizontal resolution, except in the equatorial band where the meridional resolution is 1/3°. The initial conditions for the atmosphere were obtained from operational analyses. The initial conditions for the ocean came from three different DA systems. One system is based on a four-dimensional variational scheme assimilating surface and subsurface thermal data and is forced by winds produced from NMC analyses. The other two systems insert only SST data and are forced by NMC winds and atmospheric model winds. The model winds were derived by running the atmospheric model with observed SST as the boundary forcing, thus initializing the ocean using only SST data. All three DA systems were run out over the period 1981–88, storing the ocean state for each month. The space–time evolution of the upper ocean heat content was quite different between the three DA schemes. However, the anomaly patterns were similar showing the natural mode of oscillation of the tropical Pacific air–sea system. This so-called delayed oscillator mode is characterized by eastward propagation along the equatorial waveguide and westward propagation off the equator. The implication here is that

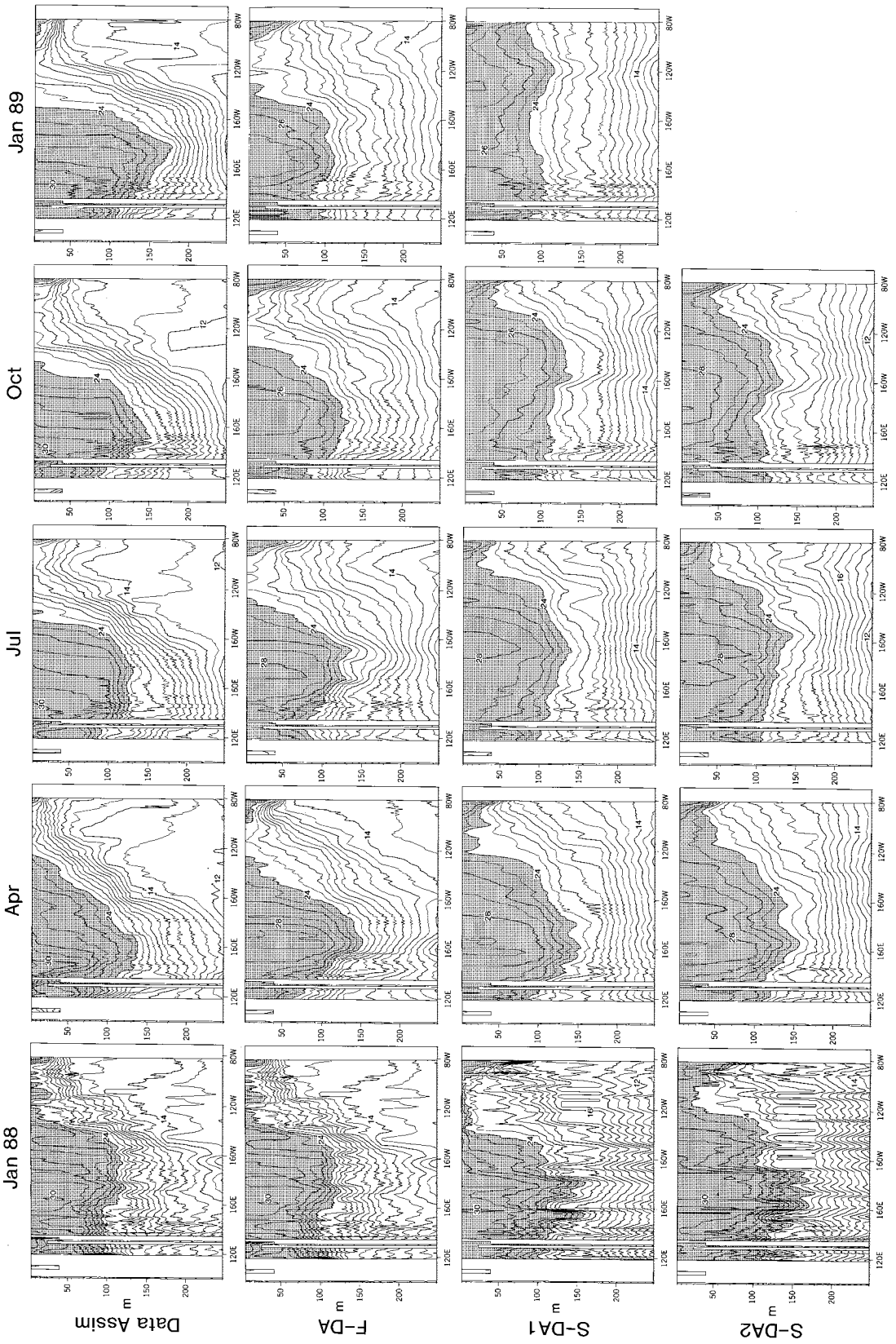

FIG. 14. The same as Fig. 10 but for 1988.

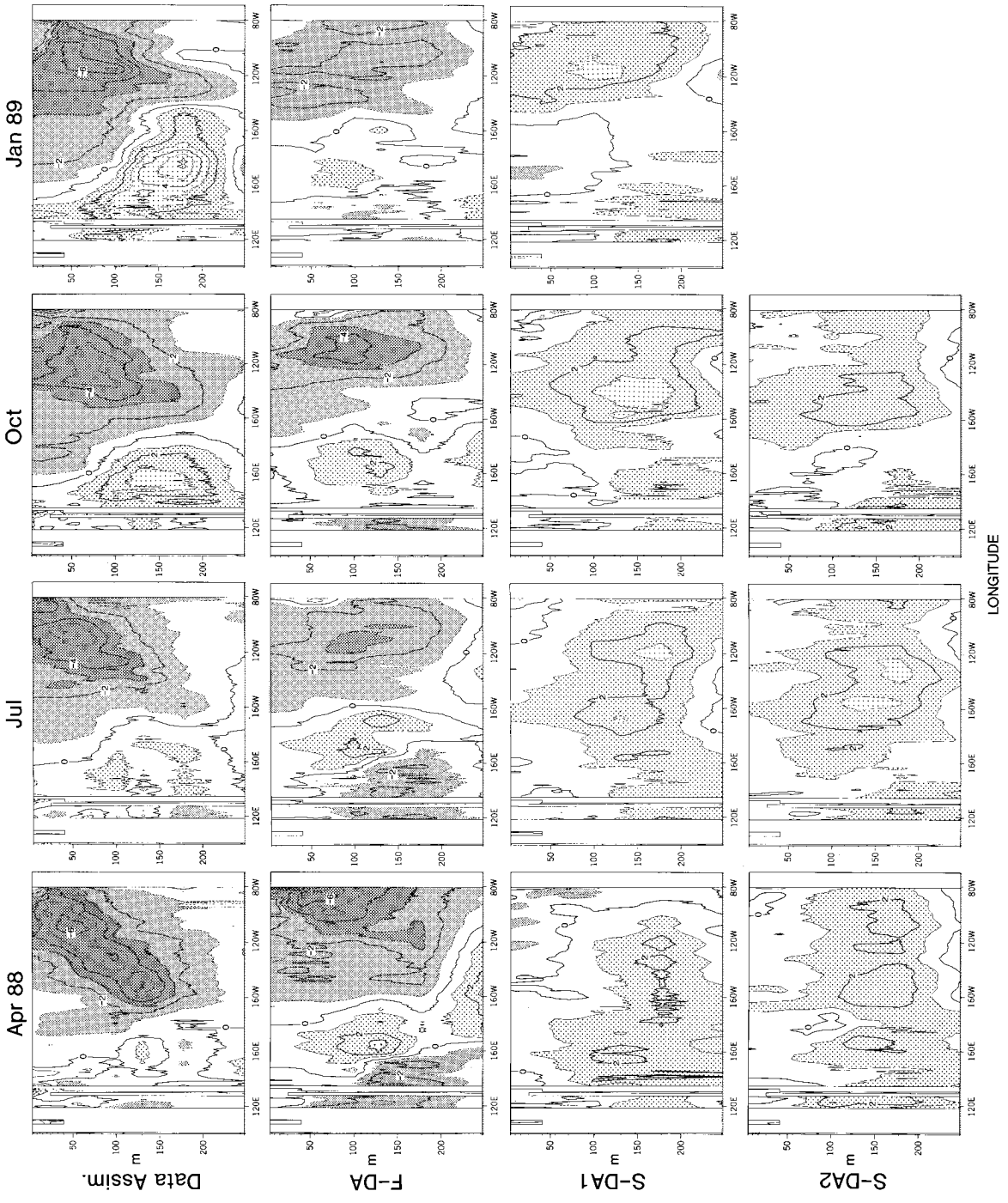

FIG. 15. The same as Fig. 11 but for 1988.

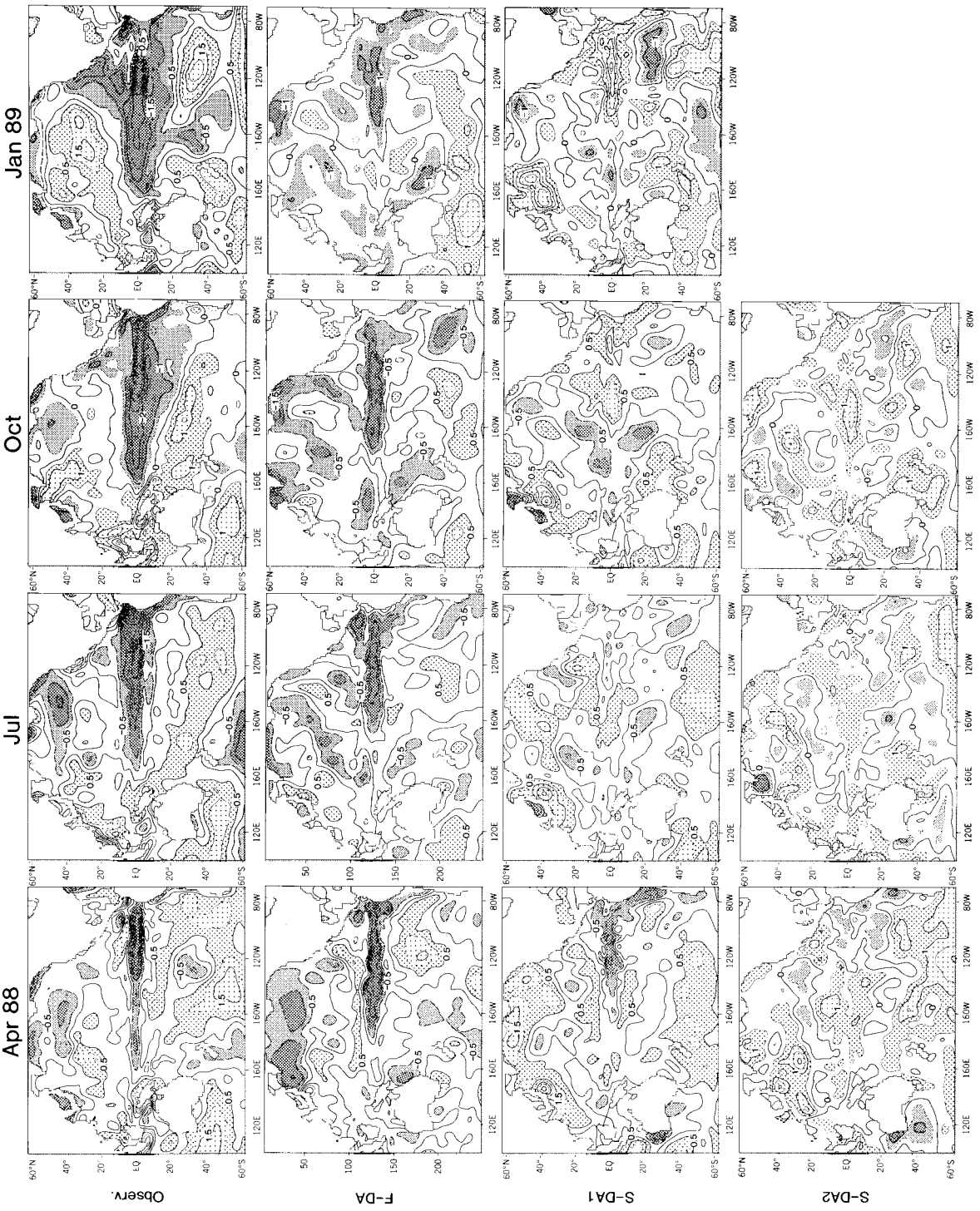

FIG. 16. The same as Fig. 12 but for 1988.

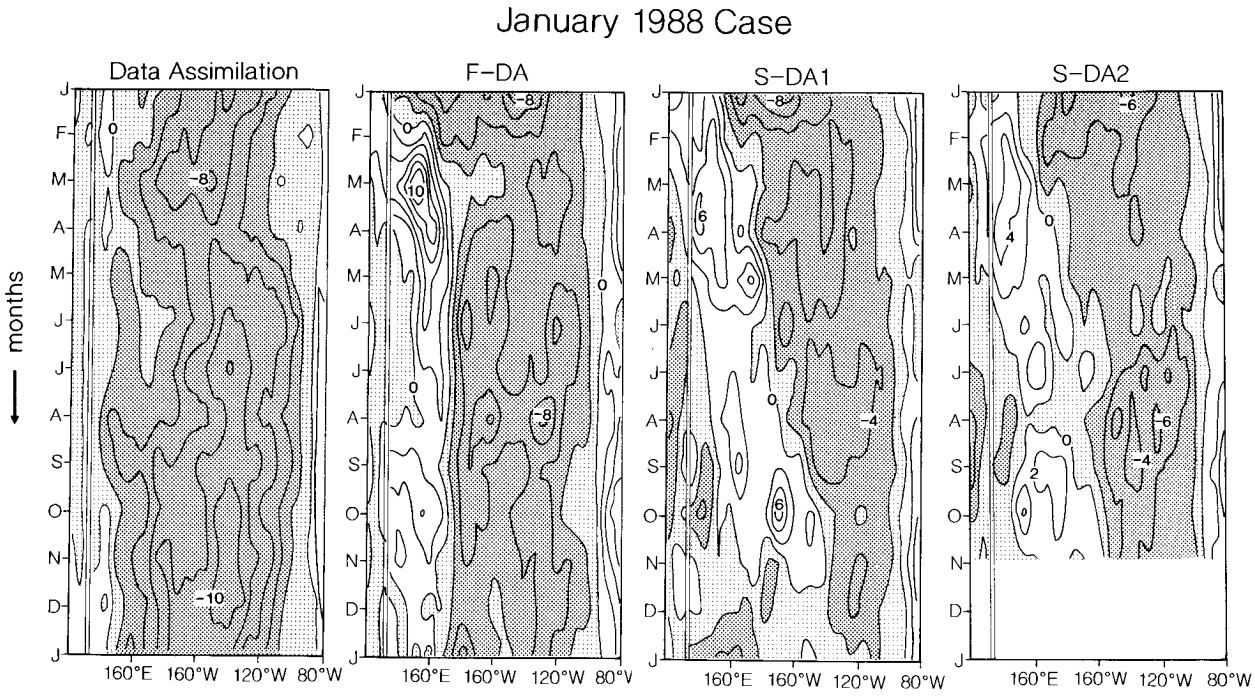

FIG. 17. The same as Fig. 13 but for 1988.

the wave dynamics of the ocean model and the wind forcing may produce reasonable propagation of anomalous thermocline displacements, but the total heat distribution could be quite different without being constrained by subsurface observations.

The coupled model was used to make 13-month forecasts for seven January and seven July cases. Analysis of the results of these forecasts led to the following conclusions.

1) Focusing the discussion on forecasting Nino-3 SST anomalies, it was found that the F-DA forecasts, whose ocean initial conditions were based on a DA scheme that contained subsurface thermal data, demonstrated the most skill. Preconditioning the initial ocean state only from surface data, S-DA cases, did not produce results as good as the F-DA cases. The issue of seasonality was addressed by forecasting from winter and summer. The January cases showed remarkably good skill for the whole 13-month period. The July cases also showed good skill, until a marked decline after eight months, beginning in the spring.

These results show the importance of correctly representing the initial state of the ocean for ENSO prediction. Perhaps the failure of the S-DA cases is that the ocean model, without subsurface data inserted, tends toward a thermocline that is too diffuse. This tendency could alter the response of the SST to thermocline changes since the subsurface information would be disconnected from the surface.

2) Despite the climate drift exhibited by the coupled model in simulating the tropical Pacific annual cycle, the F-DA SST anomaly forecasts showed considerable skill. The presence or absence of interannual variability does not appear to depend importantly on the model's climate drift. It is expected that, in order to improve the model's forecast skill for atmospheric quantities in the extratropics, the annual cycle must be improved.

The capricious nature of the coupled GCM system makes it difficult to make improvements in the model physics that are robust in their reduction of systematic error and not just different. Subsequent improvements of the atmospheric model have led to reducing the coupled model's climate drift but this work is ongoing research. With the advent of new ocean datasets (i.e., satellite altimetry, TOGA–TAO array of moorings), the ocean initial conditions from DA analysis may be substantially improved. As each of the components of the air–sea coupled system improves, so do the prospects of improving seasonal forecasts.

Acknowledgments. We would like to thank Drs. J. Anderson, D. Gu, G. Lau, and J. Mahlman for their critical comments on the manuscript. Special thanks go to Ms. Cathy Raphael, Mr. J. Varanyak, and Ms. W. Marshall, who drafted the figures and prepared the manuscript.

REFERENCES

Anderson, D. L. T., and A. M. Moore, 1989: Initialization of equatorial waves in ocean models. *J. Phys. Oceanogr.*, **19,** 116–121.

Arpe, K., A. Hollingsworth, M. S. Tracton, A. C. Lorenc, S. Uppala,

and P. Kallberg, 1985: The response of numerical weather prediction systems to FGGE level IIb data. Part II: Forecast verifications and implications for predictability. *Quart. J. Roy. Meteor. Soc.,* **111,** 67–101.

Barnett, T. P., M. Latif, E. Kirk, and E. Roeckner, 1991: On ENSO physics. *J. Climate,* **4,** 487–515.

——, ——, N. Graham, M. Flugel, S. Pazan, and W. White, 1993: ENSO and ENSO-related predictability. Part I: Prediction of equatorial Pacific sea surface temperature with a hybrid coupled ocean–atmosphere model. *J. Climate,* **6,** 1545–1566.

Battisti, D. S., 1988: Dynamics and thermodynamics of a warming event in a coupled tropical atmosphere–ocean model. *J. Atmos. Sci.,* **45,** 2889–2919.

Blumenthal, M. B., 1991: Predictability of a coupled ocean–atmosphere model *J. Climate,* **4,** 766–784.

Bryan, K., 1969: A numerical method for the study of the World Ocean. *J. Comput. Phys.,* **4,** 347–376.

Busalacchi, A. J., and J. J. O'Brien, 1980: The seasonal variability in a model of the tropical Pacific. *J. Phys. Oceanogr.,* **10,** 1929–1951.

——, K. Takeuchi, and J. J. O'Brien, 1983: Interannual variability of the equatorial Pacific revisited. *J. Geophys. Res.,* **88,** 7531–7562.

Cane, M. A., S. E. Zebiak, and S. C. Dolan, 1986: Experimental forecasts of El Niño. *Nature,* **321,** 827–832.

Chao, Y., and S. G. H. Philander, 1993: On the structure of the Southern Oscillation. *J. Climate,* **6,** 450–469.

Chen, D., S. Zebiak, M. Cane, and A. Busalacchi, 1997: Initialization and predictability of a coupled ENSO forecast model. *Mon. Wea. Rev,* **125,** 773–788.

Cox, M. D., 1984: A primitive equation, 3-dimensional model of the ocean. GFDL Ocean Group. Tech. Rep. No. 1, 143 pp. [Available from GFDL, Box 308, Princeton, NJ 08542.]

Derber, J., and A. Rosati, 1989: A global oceanic data assimilation system. *J. Phys. Oceanogr.,* **19,** 1333–1347.

Gandin, L. S., 1963: *Objective Analysis of Meteorological Fields.* Gidromet, 242 pp.

Gordon, C. T., 1992: Comparison of 30-day integration with and without cloud-radiation interaction. *Mon. Wea. Rev.,* **120,** 1244–1277.

——, and W. F. Stern, 1982: A description of the GFDL global spectral model. *Mon. Wea. Rev.,* **110,** 625–644.

Graham, N. E., and W. B. White, 1988: The El Niño cycle: A natural oscillator of the Pacific Ocean–atmosphere system. *Science,* **240,** 1293–1302.

Hao, Z., and M. Ghil, 1994: Data assimilation in a simple tropical ocean model with wind stress errors. *J. Phys. Oceanogr.,* **24,** 2111–2128.

Harrison, D. E., 1989: Local and remote forcing of ENSO ocean waveguide response. *J. Phys. Oceanogr.,* **19,** 691–693.

Inoue, M., and J. J. O'Brien, 1984: A forecasting model for the onset of El Niño. *Mon. Wea. Rev.,* **112,** 2326–2337.

Ji, M., and T. Smith, 1995: Ocean model response to temperature data assimilation and varying surface wind stress: Intercomparisons and implications for climate forecast. *Mon. Wea. Rev.,* **123,** 1811–1821.

——, A. Kumar, and A. Leetmaa, 1994: An experimental coupled forecast system at the National Meteorological Center: Some early results. *Tellus,* **46A,** 398–418.

Latif, M., 1987: Tropical ocean circulation experiments. *J. Phys. Oceanogr.,* **17,** 246–263.

——, and M. Flugel, 1991: An investigation of short range climate predictability in the tropical Pacific. *J. Geophys. Res.,* **96**(C2), 2661–2673.

——, and N. E. Graham, 1992: How much predictive skill is contained in the thermal structure of an OGCM. *J. Phys. Oceanogr.,* **22,** 951–962.

——, A. Sterl, E. Maier–Reimer, and M. M. Jaye, 1993: Structure and predictability of the El Niño–Southern Oscillation phenomenon in a coupled GCM. *J. Climate,* **6,** 700–708.

Lau, N-C, 1985: Modeling the seasonal dependence of the atmosphere response to observed El Niños in 1962–76. *Mon. Wea. Rev.,* **113,** 1970–1996.

Mellor, G. L., and T. Yamada, 1974: A hierarchy of turbulent closure models for planetary boundary layers. *J. Atmos. Sci.,* **31,** 1791–1806.

Miyakoda, K., J. Sirutis, A. Rosati, and R. Gudgel, 1989: Some activities at GFDL relevant to COARE. *Proc. Workshop on Japanese-Coupled Ocean Atmosphere Response Experiments,* 93–104.

——, ——, ——, and J. Derber, 1990: Experimental seasonal forecasts with an air–sea model—Preliminary results. *Air–Sea Interaction in Tropical Western Pacific,* J.-P. Chao and J. A. Young, Eds., China Press, 417–432.

Navarra, A., W. F. Stern, and K. Miyakoda, 1994: Reduction of Gibbs oscillation in spectral model simulation. *J. Climate,* **7,** 1169–1183.

Neelin, J. D., and Coauthors, 1992: Tropical air–sea interaction in general circulation models. *Climate. Dyn.,* **7,** 75–104.

Pacanowski, R. C., K. Dixon, and A. Rosati, 1991: The GFDL Modular Ocean Model users guide, Version 1.0. GFDL Ocean Group. Tech. Rep. No. 2. [Available from GFDL, Box 308, Princeton, NJ 08542.]

Philander, S. G. H., and A. D. Seigel, 1985: Simulation of El Niño of 1982–1983. *Coupled Ocean–Atmosphere Models,* J. G. J. Nihoul, Ed., Elsevier Oceanography Series, Vol. 40, 517–541.

——, W. J. Hurlin, and R. C. Pacanowski, 1987: Initial conditions for a general circulation model of tropical ocean. *J. Phys. Oceanogr.,* **17,** 147–157.

Reynolds, R. W., 1982: A monthly averaged climatology of sea surface temperature. NOAA Tech. Rep. NWS 31, 33 pp.

——, 1988: A real time global sea surface temperature analysis. *J. Climate,* **1,** 75–86.

Rosati, A., and K. Miyakoda, 1988: A general circulation model for upper ocean circulation. *J. Phys. Oceanogr.,* **18,** 1601–1626.

——, R. Gudgel, and K. Miyakoda, 1994: Decadal analysis produced from an ocean data assimilation system. *Mon. Wea. Rev.,* **123,** 2206–2228.

Schopf, P. S., and M. J. Suarez, 1988: Vacillations in a coupled ocean–atmosphere model. *J. Atmos. Sci,* **45,** 549–566.

Sirutis, J., and K. Miyakoda, 1990: Subgrid scale physics in 1-month forecasts. Part I: Experiment with four parameterization packages. *Mon. Wea. Rev.,* **118,** 1043–1064.

Smagorinsky, J., 1963: General circulation experiments with the primitive equations. Part I: The basic experiment. *Mon. Wea. Rev.,* **91,** 99–164.

Stern, W. F., and K. Miyakoda, 1989: Systematic errors in GFDL's extended range prediction spectral GCM. *Proc. Workshop on Systematic Errors in Models of the Atmosphere,* 136–140.

——, and ——, 1995: Feasibility of seasonal forecasts inferred from multiple GCM simulations *J. Climate,* **8,** 1071–1085.

Wyrtki, K., 1985: Water displacements in the Pacific and the genesis of El Niño cycles. *J. Geophys. Res.,* **90**(C4), 7129–7132.

Zebiak, S., and M. A. Cane, 1987: A model El Niño–Southern Oscillation. *Mon. Wea. Rev.,* **115,** 2262–2278.